

CrystEngComm

Accepted Manuscript

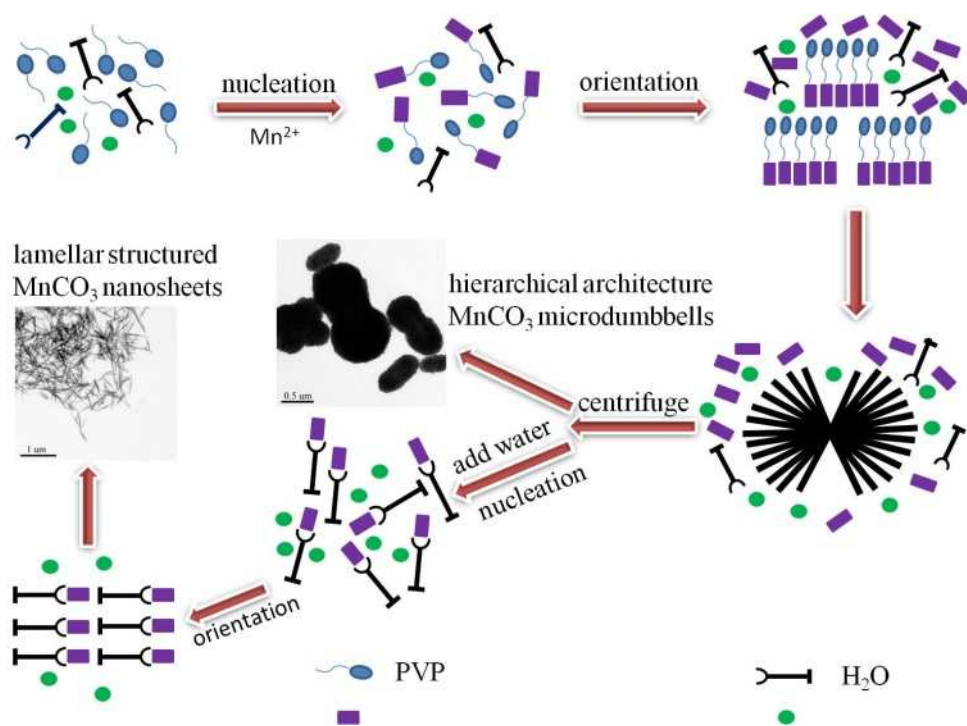


This is an *Accepted Manuscript*, which has been through the Royal Society of Chemistry peer review process and has been accepted for publication.

Accepted Manuscripts are published online shortly after acceptance, before technical editing, formatting and proof reading. Using this free service, authors can make their results available to the community, in citable form, before we publish the edited article. We will replace this *Accepted Manuscript* with the edited and formatted *Advance Article* as soon as it is available.

You can find more information about *Accepted Manuscripts* in the [Information for Authors](#).

Please note that technical editing may introduce minor changes to the text and/or graphics, which may alter content. The journal's standard [Terms & Conditions](#) and the [Ethical guidelines](#) still apply. In no event shall the Royal Society of Chemistry be held responsible for any errors or omissions in this *Accepted Manuscript* or any consequences arising from the use of any information it contains.





Hierarchical architecture MnCO₃ microdumbbells: Facile synthesis and enhanced performance for lithium ion batteries

Received 00th January 20xx,
Accepted 00th January 20xx

DOI: 10.1039/x0xx00000x

www.rsc.org/

Liu Zhang, Tao Mei*, Xianbao Wang, Jianying Wang, Jinhua Li, Weilai Xiong, Yi Chen, Ming Hao

Hierarchical architecture MnCO₃ microdumbbells and lamellar structured MnCO₃ nanosheets were selectively synthesized by a facile reflux route. Hierarchical architecture MnCO₃ microdumbbells (approximately 0.5–1.5 μm in length and 0.3–0.9 μm in width) were comprised of nanoparticles, while the lamellar structured MnCO₃ nanosheets had uniform length of approximate 400 nm. Both of them were employed as anode active materials in lithium ion batteries. Experiment results showed that the hierarchical architecture MnCO₃ microdumbbells exhibited superior electrochemical performances compared with the lamellar structured MnCO₃ nanosheets. At a current rate of 0.5 C, the reversible capacity of hierarchical architecture MnCO₃ microdumbbells electrode after 100 cycles was 775 mAh g⁻¹, while the lamellar structured MnCO₃ nanosheets was only 50 mAh g⁻¹ left after 100 cycles. The superior electrochemical behavior of hierarchical architecture MnCO₃ microdumbbells materials could be ascribed to the unique micro-nano assembly structure, simultaneously cushioning the volume change, maintaining the electrode integrity and offering short diffusion distance.

1. Introduction

lithium-ion batteries (LIBs), in the near future, show promising application as power sources for electric vehicles (EVs) and hybrid electric vehicles (HEVs)¹. To satisfy the growing appetite for these applications, further improvements in terms of energy and power densities, safety, cost, and lifetime are taken into consideration². Nevertheless, the commercial graphite-based anode materials cannot meet the burgeoning requirements in the virtue of limited specific capacity and low power density³. In this respect, manifold anode materials have been explored as an essential constituent in LIBs, such as Si, transition-metal oxides, and their analogues^{4–7}. As an important conversion-type material, manganese carbonate (MnCO₃) is considered to be an potential anode materials due to its high nature abundance, low toxicity, low cost as well as high theoretic Li-storage capacity (467 mAh g⁻¹), which exceeds the traditional graphite anode material (the theoretic capacity is 372 mAh g⁻¹). Particularly, MnCO₃ materials are widely used as sacrificial templates to synthesize its respective derivative metal oxides via thermal conversion with the target morphologies^{8–11}. In general, the shape guiding-mechanism leaves the MnCO₃ an unavoidable hot topic. However, because of large volume change during delithiation/lithiation processes and the inherent low conductivity of these

carbonates, MnCO₃ suffers from unwanted capacity fading, which hinders the development of these materials^{3,12}.

To address these problems, many efforts have been made, such as designing unique morphologies and the introduction of nanosized materials, because the electrochemical performance of the electrode materials are to some degree associated with size dimension, structure as well as crystalline orientation, namely the morphology¹³. Nanostructured materials shorten diffusion distance to some extent, which may appears to be a hot research field for the great potential in terms of space-confined transport phenomena as well as applications. Furthermore, there are a variety of techniques to synthesize MnCO₃ micro/nanostructures, including chemical precipitation method^{14–18}, hydrothermal and solvothermal routes^{19–23}, ultrasonic^{24, 25}, and micelle method^{26, 27}. For example, a pseudo-square shaped MnCO₃ was synthesized via a reverse micelles method, which exhibited a capacity of 372 mAh g⁻¹ at 2 C²⁸. Zhou and co-workers³ fabricated a MnCO₃@rGO composite by attaching MnCO₃ nanoparticles to rGO sheets through hydrothermal method, which obtained high capacity to 857 mAh g⁻¹ after 100 cycles at a current rate of 0.2 C. Moreover, a facile precipitation technique was used to prepare MnCO₃/CNT nanocomposites, which showed the capacity of 647 mAh g⁻¹ at a current density of 100 mA g⁻¹ after 100 cycles¹².

Among them, the synthesis of MnCO₃ nanostructures with multi-morphology nanoparticles usually require complex preparation processes or the presence of surfactants, leading to the increased production cost and impurities, which embarrass the application of MnCO₃ in batteries. On the other hand, for the nanosized materials there is a trend to agglomerate together, and enhance the side reaction with electrolyte, owing to the large active sites of these materials²⁹. Therefore, the development of a effective, simple, and

Hubei Collaborative Innovation Center for Advanced Organic Chemical Materials, Ministry of Education, Key Laboratory for the Green Preparation and Application of Functional Materials, School of Materials Science and Engineering, Hubei University, Wuhan 430062, PR China. E-mail: meitao@hubu.edu.cn; Fax: +86-27-8866-1729; Tel: +86-27-8866-2132

environmental friendly route to prepare MnCO_3 micro-nano assembly structure, which maintain the electrode integrity and cushion the volume change, is still urgent for meeting the demand of pushing the research forward. Herein, in this work, we report a refluxing and subsequent heating under lower temperature method to selectively synthesize the hierarchical architecture MnCO_3 microdumbbells and two-dimensional (2D) lamellar structured MnCO_3 nanosheets. The hierarchical architecture MnCO_3 microdumbbells simultaneously holds the advantages of nanosized and microsized materials, namely cushioning the volume change, maintaining the electrode integrity and offering short diffusion distance, benefiting from myriad tunnels among nanoparticles. As an anode active materials in lithium ion batteries, the hierarchical architecture MnCO_3 microdumbbells electrode could deliver a reversible capacity of 583, 463, 397, 399, 262 mAh g^{-1} at a current rate of 0.2 C, 0.5 C, 1C, 2 C and 5 C. At a reverted rate of 0.2 C, a high capacity up to 697 mAh g^{-1} was obtained and remained steadily ascending.

2. Experimental Section

2.1 Synthesis of MnCO_3 microdumbbells

The schematic illustration of the reaction process is given in Scheme 1. All the chemical reagents used here were analytical grade, and without further purification. In a typical synthesis, $\text{Mn}(\text{NO}_3)_2$ (50 wt.% solution, 2 mL), urea (0.5 g), and poly(vinyl pyrrolidone) (PVP, K-30; 0.4 g) and ethylene glycol (EG; 50 mL) were mixed by magnetic stirring until it went to clear solution, which was then heated to a refluxing temperature (ca. 150 °C). After refluxing for 2 hours, we got a dark brown solution. The white precipitate and a dark brown solution were separated by centrifugation for once. Then, the white precipitate was washed thoroughly with water and absolute ethanol for several times, proved to be hierarchical architecture MnCO_3 microdumbbells in the results and discussion part.

2.2 Synthesis of lamellar structured MnCO_3 nanosheets

It is noted that while the dark brown solution was heated to about 70 °C in air for several minutes. Then, a brown flocculent precipitate began to appear, indicating the formation of lamellar structured MnCO_3 nanosheets. The as-synthesized brown flocculent precipitate was washed with water and absolute ethanol for several times to remove impurities, and then dried in vacuum oven at 60 °C for 12 h.

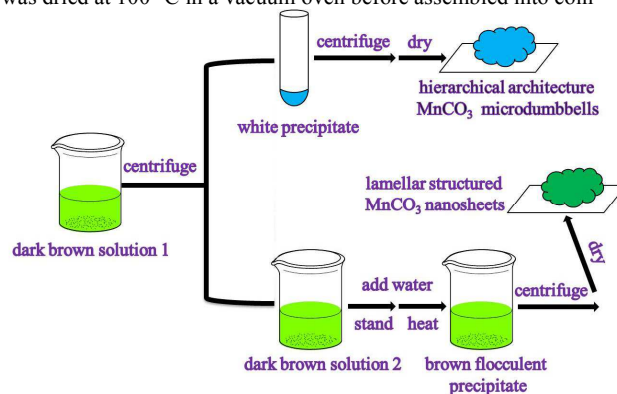
2.3 Structure Characterizations

The phase of two as-synthesized products were characterized by power X-ray diffraction (XRD; Bruker, Germany) with a Cu $K\alpha$ radiation source ($\lambda=0.15418$ nm) operated at 40 kV and 40 mA. Morphology and microstructure of the products were characterized by field-emission scanning electron microscopy (SEM; ZEISS, Germany) and transmission electron microscopy (TEM; FEI TECNAI20, USA). The surface area and porous structures of the two products were tested by nitrogen adsorption-desorption (QDS-MP-30) at 77 K.

2.4 Electrochemical measurements

Electrochemical performances were evaluated with CR2016 coin type cells. The coin cells were comprised of the manganese carbonate cathode, a metallic lithium anode, 1 M LiPF_6 in a 1:2 ethylene carbonate/diethyl carbonate electrolyte, and a Celgard 2400 separator. To prepare the cathode, active material, super P Li conductive carbon black, and polyvinylidene fluoride (PVDF) were mixed by the weight ratio of 70:20:10 with N-methyl pyrrolidone

(NMP), coating the resulting slurry onto aluminum foil, the cathode was dried at 100 °C in a vacuum oven before assembled into coin



Scheme 1. Schematic illustration of the reaction processes.

cell in an argon-filled glove box. All coin cells were cycled using a Land battery Test System (Wuhan, China). The assembled cells were charged and discharged within the voltage range of 0.001-3.0 V at a varieties of current density at room temperature. The final capacities were calculated based on the weight of the MnCO_3 . Cyclic voltammetry (CV) was launched between 0.001 and 3 V at the scanning rate of 0.1 mV/s, and electrochemical impedance spectroscopy (EIS) data was recorded using a CHI 760E electrochemical workstation.

3. Results and discussion

Figure 1a showed XRD pattern of the white product synthesized at the temperature of 150 °C just by refluxing without any other further heating treatment. The sharp and high intensity peaks could be well fitted to the rhombohedral phase of MnCO_3 (JCPDS Card No. 44-1472) under R-3c space group, thus verifying that the as-obtained compounds held the proper crystallinity without impurity. The particle size and morphology of MnCO_3 sample were shown in Figure 1b. It displayed the microdumbbell shaped hierarchical architecture (approximately 0.5-1.5 μm in length and 0.3-0.9 μm in width), consisted of massive nanoparticles, which was consistent with the TEM images showed in Figure 1c. Specially, there were the four-leaf clover-like particles as marked by the red rectangle in Figure 1c, probably resulting from a couple of aggregating hierarchical architecture MnCO_3 microdumbbells. Furthermore, as shown in Figure 1d, the microdumbbells were consisted of massive nanoparticles, leading to the formation of the myriad tunnels among nanoparticles, the surface of the as-obtained sample was not smooth, and turned out to be zigzag, resulting in larger specific surface area compared with the smooth one. On the other hand, it was beneficial to increase the active sites, promote the Li^+ ion intercalation/deintercalation during charge/discharge process.

It was interesting to figure out that the flocculent precipitate had a quite different morphology compared with the hierarchical architecture MnCO_3 microdumbbells product. The lamellar structure of flocculent precipitate could be clearly observed (Figure 2). As seen from these images, the well-distributed lamellar morphology had uniform aspect, irregular sheet-shape with length of approximate 400 nm, and a tendency to come out wrinkled. It was likely that the primary lamellars tended to grow laterally along the nanosheets, which was due to the recrystallization during the Ostwald ripening process^{30, 31}. The structure and phase transformations were directly confirmed by XRD characterizations, and Figure 2a showed the power XRD pattern of the lamellar structured MnCO_3 nanosheets. All of the peaks confirmed that the lamellar structured MnCO_3

nanosheets could be indexed to the rhombohedral phased MnCO_3 (JCPDS Card No. 44-1472), which was the same phase with the hierarchical architecture MnCO_3 microdumbbells discussed above. However, the broadened diffraction peaks suggested that the crystallinity of the lamellar structured MnCO_3 nanosheets was poor, and the crystalline sizes of the as-obtained MnCO_3 might be in nanometer scale, which was consistent with the TEM images showed in Figure 2d.

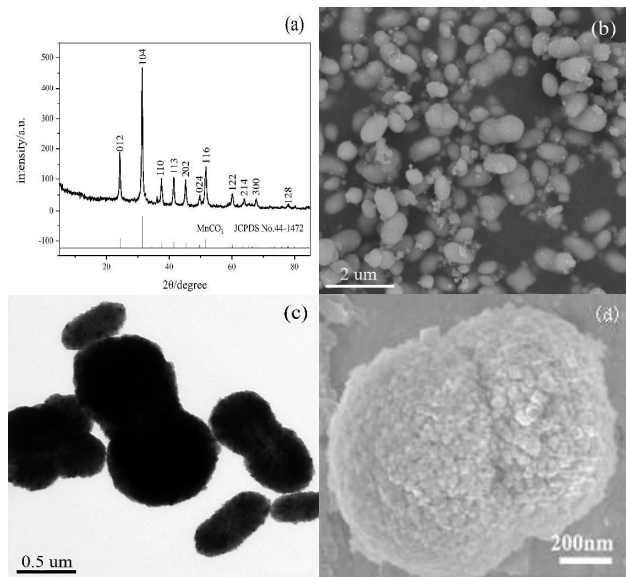


Figure 1. (a) XRD pattern of the hierarchical architecture MnCO_3 microdumbbells, (b),(c) and (d) the corresponding SEM and TEM images, respectively.

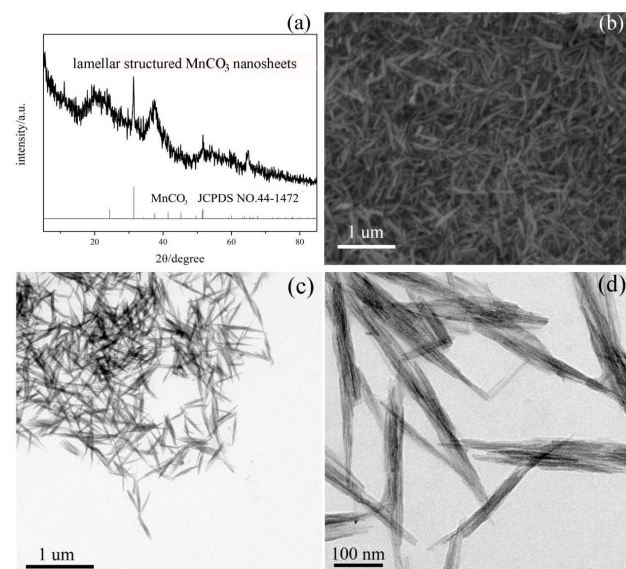


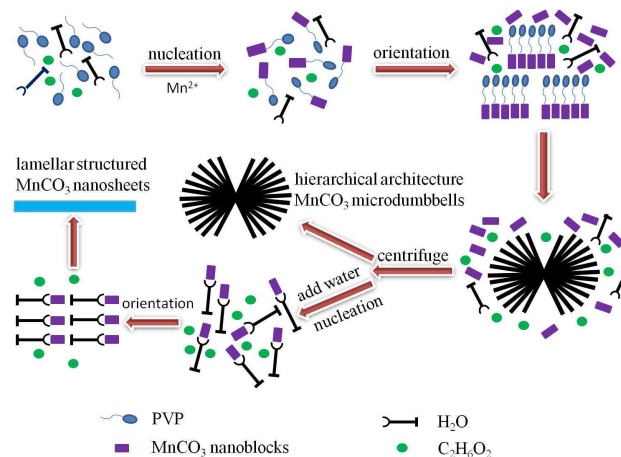
Figure 2. (a) XRD pattern of the lamellar structured MnCO_3 nanosheets, (b),(c) and (d) the corresponding SEM and TEM images, respectively.

As the respect of mechanism, it is well known that the growth of organic colloids by precipitation reactions involves nucleation and

the subsequent growth of the nuclei³². During this crystal growth process, organic ligands play significant important roles. These ligands selectively attach onto the surface of the nuclei, serving as templates, coordinating with nuclei and metal ions in specific geometry¹⁴ and suitable speed of crystal growth. In this paper, we will propose the conceivable mechanism (Scheme 2). According to the reactants, the formation of MnCO_3 nuclei may be described as the following steps:

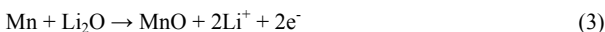
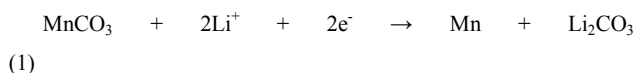


At the initial nucleating stage, the MnCO_3 nuclei form through the reaction between Mn^{2+} and CO_3^{2-} , and tend to form nanoblocks due to the crystal nature of rhombohedral structure³³. During the crystal growth stage, the nanoblocks are capped with organic colloids, and subsequently follow the orientated attachment according to the geometry and strength of the organic colloids^{20, 34}. As a result, the hierarchical architecture MnCO_3 microdumbbells are generated. Meanwhile, after adding water to the dark brown solution, the water molecules are selectively adsorbed on the certain surface facets of residual MnCO_3 nuclei, and the particles self-assemble along the same axis to form a basic sheet unit through orientation growth. We have to point out that the basic sheet unit tended to grow laterally along the nanosheets due to the recrystallization during the Ostwald ripening process, which have been mentioned above.



Scheme 2. Schematic illustration on the formation processes of the as-obtained two MnCO_3 production.

Considering about Li storage mechanism of conversion materials, it could be said that during discharge process of the manganese carbonate, the active materials decomposed to Mn^0 and Li_2CO_3 followed by partial reduction of Li_2CO_3 into Li_2O ³⁵⁻³⁸. On the contrary, the metallic Mn participated in the oxidation reaction, leading to the recovery of the manganese oxide. Generable speaking, the charge/discharge processes entailed a reversible Li-driven decomposition of the metal carbonate into a composite matrix comprised of metallic inorganic nanoparticles dispersed into a Li_2O medium, similar to the carbon-base electrodes³⁸. Subsequently, it was easy to understand that there is a capacity increase for the cycling profile, which was similar to many pure conversion materials^{35, 39}, and it showed in Figure 3a. These multistep reactions can be written as the following⁴⁰.



With the aim to distinguish the outstanding Li-storage behaviors between the two MnCO₃ productions, Figure 3a showed the cyclic performance at a current rate of 0.5 C. The initial discharge capacity reached 1411 mAh g⁻¹ and remained 775 mAh g⁻¹ after 100 cycles for the hierarchical architecture MnCO₃ microdumbbells. Obviously, the reversible capacity greatly exceeded the theoretic value (467 mAh g⁻¹), which might be ascribed to the Faradaic contributions of side reaction, the irreversible formation of SEI layer, and the pseudocapacitance-type behavior of the electrode material^{7, 41, 42}. Meanwhile, the lamellar structured MnCO₃ nanosheets materials displayed a much lower capacity, and a considerable capacity fading compared with the hierarchical architecture MnCO₃ microdumbbells materials. The outperformance of hierarchical architecture MnCO₃ microdumbbells materials could be attributed to the unique micro-nano assembly structure. Firstly, a large number of interspace among nanoparticles consisted of microdumbbells provided the varied electron and Li⁺ transport channels, boosted the rapid diffusion of electrons and ions. Then, the hierarchical structure could accommodate the volume swings in comparison with the lamellar structured MnCO₃ nanosheets materials during the repeated charge-discharge processes. To better understand the electrochemical performance of hierarchical architecture MnCO₃ microdumbbells, galvanostatic measurements were conducted at a current rate of 0.5 C (Figure 3b) and the charge-discharge results along with the corresponding CV profiles were showed in Figure 3c. In the initial discharge profile, the voltage value rapidly fell to the plateau of 0.25 V, which might owe to the reduction from MnCO₃ to Mn (eq. (1)). Then, it gradually descended to the cut-off voltage (0.01V). As for the second discharge curve, the voltage value of plateau was approximately 0.5 V, which might be attributed to another conversion from manganese oxide to Mn (eq. (2)). The upshift took place due to the formation of SEI films in the first discharge process and the polarization of the electrode in the following cycles. Then, it became stable at a plateau of ca. 0.25-0.5 V from 50th cycle to 100th cycle. The charge/discharge performances of the as-synthesized hierarchical architecture MnCO₃ microdumbbells were analogous to the previous reports^{3, 40}. According to the CV profiles, we could see that, for the initial CV curves, the broad oxidation peak in the range from 1.05 to 2.75 V could be ascribed to the oxidation of Mn⁰ metal, and the reduction peak centered between 0.25-0.75 V could be attributed to the reduction of Mn²⁺ to Mn⁰. The reduction peak was small compared to the oxidation peak, which might owe to the obstruction of the SEI films. Therefore, the coulombic efficiency for the initial cycle was only 46.16%. But after undergoing charge/discharge processes for 50 cycles, the oxidation peak was split into two peaks at 1.35 and 2.25 V resulting from the oxidation of Mn⁰ to Mn²⁺ and the Mn²⁺ to a higher oxidation state⁴³, respectively. As for the reduction peaks, the peak centered at 0.75 V could be ascribed to the reduction of Mn²⁺, while the wave concerned at around 1.95 V was due to the reduction of high oxidation state Mn (a part of impurity) by lithium. The reduction peaks matched well compared to the oxidation peaks, which meant that the capacity retention and coulombic efficiency after 50 cycles were great, and it was in agreement with the cycling performances showed in Figure 3a. As for the rate performance, the hierarchical architecture MnCO₃ microdumbbells electrode could deliver a reversible capacity of 583, 463, 397, 399, 262 mAh g⁻¹ at a current rate of 0.2 C, 0.5 C, 1C, 2 C and 5 C (Figure 3d). At a reverted rate of 0.2 C, a high capacity up to 697 mAh g⁻¹ was obtained and remained steadily ascending. The electrochemical impedance spectra

showed in Figure 3e, displayed a semicircle at high frequency, which corresponded to the charge-transfer resistance, and a inclined line, which related to the lithium-diffusion process. It was convinced that the resistance of hierarchical architecture MnCO₃ microdumbbells materials was considerably lower than the lamellar structured MnCO₃ nanosheets materials due to the smaller half-cycle curve, namely the lower charge-transfer resistance accounting for the reasonable improvement in the kinetic performance.

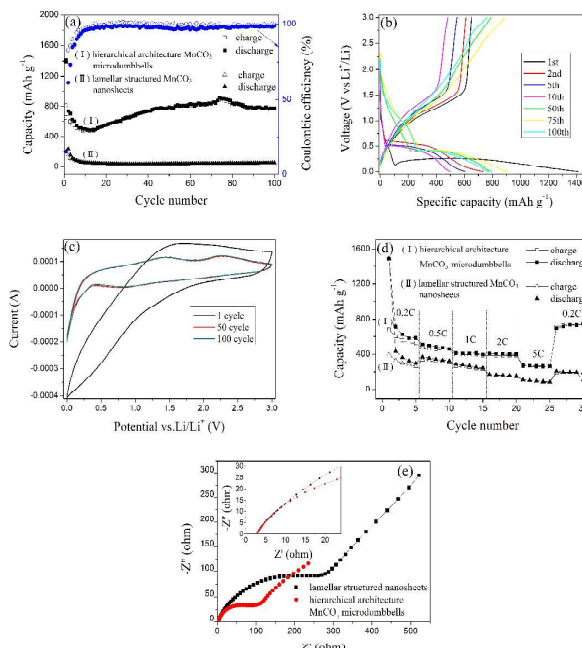


Figure 3. (a) cycling performances of the hierarchical architecture MnCO₃ microdumbbells and the lamellar structured MnCO₃ nanosheets at the current rate of 0.5 C (b) discharge-charge curves of different cycles at the current rate of 0.5 C, (c) CV plots between 0.001 and 3 V at the scanning rate of 0.1 mV/s, (d) rate performances at different current densities, (e) Nyquist profiles of the hierarchical architecture MnCO₃ microdumbbells and the lamellar structured MnCO₃ nanosheets materials.

The good performance of hierarchical architecture MnCO₃ microdumbbells electrode might also be partially derived from the suitable surface area and the narrow pore size distribution. The nitrogen adsorption-desorption curves of hierarchical architecture MnCO₃ microdumbbells and the lamellar structured MnCO₃ nanosheets materials were showed in Figure 4a and b, respectively, exhibiting the IV type profiles that both had a hysteresis loop. The BET surface area of lamellar structured MnCO₃ nanosheets materials was 40 m² g⁻¹, and pore size was widely distributed in the range from 3 to 20 nm, while the hierarchical architecture MnCO₃ microdumbbells materials possessed a little bit larger surface area of 45 m² g⁻¹, and owned a narrowly distribution of pore size. The volume and structure change of hierarchical architecture MnCO₃ microdumbbells electrode during the repeatedly cycling processes could be disciplined due to the narrowly pore size distribution, which buffered the serious capacity fading to some extent.

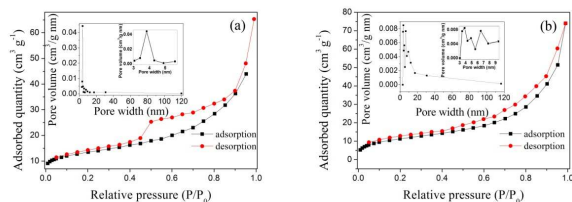


Figure 4. (a), (b) N_2 adsorption and desorption isotherms and the pore size distribution of the hierarchical architecture $MnCO_3$ microdumbbells and the lamellar structured $MnCO_3$ nanosheets, respectively.

The better electrochemical performances of hierarchical architecture $MnCO_3$ microdumbbells electrode can be ascribed to the following major factors: (a) The $MnCO_3$ micro-nano assembly structure simultaneously cushion the volume change, maintain the electrode integrity and offer short diffusion distance, deriving from the myriad tunnels among nanoparticles; (b) The high crystallinity, suitable surface area and narrow pore size distribution of the electrode materials make the surface of nanosized materials stable, which significantly enhance the capacity in terms of the cycle stability; (c) The large electron transfer rate is favorable for improving the kinetic behavior to some degree.

4. Conclusion

In summary, the two $MnCO_3$ productions with the same crystalline phase but different morphologies are prepared via a effective, simple, and environmental friendly route. Profiting from the hierarchical micro-nano assembly structure, high crystallinity, suitable surface area, narrow pore size distribution, and good conductivity, the hierarchical architecture $MnCO_3$ microdumbbells electrode exhibits high capacity, stable cycle performance, and rate capacity. This work can inspire us to develop an enhanced performance material with a unique micro-nano assembly structure.

Acknowledgements

This work was financially supported by National Natural Science Foundation (No. 21401049 and 51272071) and Hubei Provincial Department of Science & Technology (2014CFA096).

Notes and references

- G. Wang, J. Xie, C. Wu, S. Zhang, G. Cao and X. Zhao, *Journal of Power Sources*, 2014, **265**, 118-124.
- L. Zhou, D. Zhao and X. Lou, *Angewandte Chemie*, 2012, **51**, 239-241.
- L. Zhou, X. Kong, M. Gao, F. Lian, B. Li, Z. Zhou and H. Cao, *Inorganic chemistry*, 2014, **53**, 9228-9234.
- J. Cabana, L. Monconduit, D. Larcher and M. R. Palacin, *Advanced Materials*, 2010, **22**, E170-E192.
- C. K. Chan, H. Peng, G. Liu, K. Mcllwraith, X. F. Zhang, R. A. Huggins and Y. Cui, *Nature nanotechnology*, 2008, **3**, 31-35.
- K. Zhang, X. Han, Z. Hu, X. Zhang, Z. Tao and J. Chen, *Chemical Society reviews*, 2015, **44**, 699-728.
- Y. Zhong, L. Su, M. Yang, J. Wei and Z. Zhou, *ACS applied materials & interfaces*, 2013, **5**, 11212-11217.
- K. Cheng, F. Yang, G. Wang, J. Yin and D. Cao, *J. Mater. Chem. A*, 2013, **1**, 1669-1676.
- F. Dang, T. Hoshino, Y. Oaki, E. Hosono, H. Zhou and H. Imai, *Nanoscale*, 2013, **5**, 2352-2357.
- H. W. Lee, P. Muralidharan, R. Ruffo, C. M. Mari, Y. Cui and K. Kim do, *Nano letters*, 2010, **10**, 3852-3856.
- J. Li, B. Xi, Y. Zhu, Q. Li, Y. Yan and Y. Qian, *Journal of Alloys and*

Compounds, 2011, **509**, 9542-9548.

- F. Zhang, R. Zhang, G. Liang, J. Feng, L. Lu and Y. Qian, *Materials Letters*, 2013, **111**, 165-168.
- Z. Chen, R. Zhao, P. Du, H. Hu, T. Wang, L. Zhu and H. Chen, *Journal of Materials Chemistry A*, 2014, **2**, 12835.
- X.-F. Chen, L. Qie, L.-L. Zhang, W.-X. Zhang and Y.-H. Huang, *Journal of Alloys and Compounds*, 2013, **559**, 5-10.
- H. Li, X. Zhang, R. Ding, L. Qi and H. Wang, *Electrochimica Acta*, 2013, **108**, 497-505.
- X. Liu, D. Li, Q. Mo, X. Guo, X. Yang, G. Chen and S. Zhong, *Journal of Alloys and Compounds*, 2014, **609**, 54-59.
- S. M. Pourmortazavi, M. Rahimi-Nasrabadi, A. A. Davoudi-Dehaghani, A. Javidan, M. M. Zahedi and S. S. Hajimirsadeghi, *Materials Research Bulletin*, 2012, **47**, 1045-1050.
- C. Zhu, G. Saito and T. Akiyama, *Journal of Materials Chemistry A*, 2013, **1**, 7077.
- L. Cui, M. Niu, G. Chen and Y. Wang, *Materials Letters*, 2009, **63**, 2499-2502.
- X. Duan, J. Lian, J. Ma, T. Kim and W. Zheng, *Crystal Growth & Design*, 2010, **10**, 4449-4455.
- S. Lei, Z. Liang, L. Zhou and K. Tang, *Materials Chemistry and Physics*, 2009, **113**, 445-450.
- Z. Li, J. Xu, X. Chen, Q. Zhou and T. Shang, *Colloid and Polymer Science*, 2011, **289**, 1643-1651.
- L.-X. Yang, Y. Liang, H. Chen, Y.-F. Meng and W. Jiang, *Materials Research Bulletin*, 2009, **44**, 1753-1759.
- R. Cai, Y. Du, S. Peng, H. Bi, W. Zhang, D. Yang, J. Chen, T. M. Lim, H. Zhang, Y. C. Cao and Q. Yan, *Chemistry*, 2014, **20**, 421-425.
- L. X. Yang, Y. J. Zhu, H. Tong and W. W. Wang, *Ultrasonics sonochemistry*, 2007, **14**, 259-265.
- M. J. Aragón, C. Pérez-Vicente and J. L. Tirado, *Electrochemistry Communications*, 2007, **9**, 1744-1748.
- F. Pagnanelli, G. Granata, E. Moscardini and L. Toro, *Journal of Nanoparticle Research*, 2013, **15**.
- M. J. Aragón, B. León, C. Pérez Vicente and J. L. Tirado, *Journal of Power Sources*, 2011, **196**, 2863-2866.
- J. Wang, W. Lin, B. Wu and J. Zhao, *J. Mater. Chem. A*, 2014, **2**, 16434-16442.
- W. Chen, R. B. Rakhi, Q. Wang, M. N. Hedhili and H. N. Alshareef, *Advanced Functional Materials*, 2014, **24**, 3130-3143.
- T. T. Truong, Y. Liu, Y. Ren, L. Trahey and Y. Sun, *ACS Nano*, 2012, **6**, 8067-8077.
- H. Zhu, E. W. Stein, Z. Lu, Y. M. Lvov and M. J. McShane, *Chemistry of materials*, 2005, **17**, 2323-2328.
- P. Pal, S. K. Pahari, A. K. Giri, S. Pal, H. C. Bajaj and A. B. Panda, *Journal of Materials Chemistry A*, 2013, **1**, 10251.
- H. Hu, J.-y. Xu, H. Yang, J. Liang, S. Yang and H. Wu, *Materials Research Bulletin*, 2011, **46**, 1908-1915.
- Y. Zhong, L. Su, M. Yang, J. Wei and Z. Zhou, *ACS applied materials & interfaces*, 2013, **5**, 11212-11217.
- M. A. Garakani, S. Abouali, B. Zhang, C. A. Takagi, Z. L. Xu, J. Q. Huang, J. Huang and J. K. Kim, *ACS applied materials & interfaces*, 2014, **6**, 18971-18980.
- L. Wang, W. Tang, Y. Jing, L. Su and Z. Zhou, *ACS applied materials & interfaces*, 2014, **6**, 12346-12352.
- S. Laruelle, S. Grugeon, P. Poizot, M. Dollé, L. Dupont and J. M. Tarascon, *Journal of The Electrochemical Society*, 2002, **149**, A627.
- P. Poizot, S. Laruelle, S. Grugeon, L. Dupont and J. Tarascon, *Nature*, 2000, **407**, 496-499.
- G. Huang, S. Xu, Y. Yang, H. Sun, Z. Li, Q. Chen and S. Lu, *Materials Letters*, 2014, **131**, 236-239.
- M. A. Garakani, S. Abouali, B. Zhang, C. A. Takagi, Z. L. Xu, J. Q. Huang, J. Huang and J. K. Kim, *ACS applied materials & interfaces*, 2014, **6**, 18971-18980.
- L. Wang, W. Tang, Y. Jing, L. Su and Z. Zhou, *ACS applied materials & interfaces*, 2014, **6**, 12346-12352.
- S. Zhang, L. Zhu, H. Song, X. Chen and J. Zhou, *Nano Energy*, 2014, **10**, 172-180.